Translational Oncology

www.transonc.com

Volume 3 Number 1 February 2010 pp. 56–64 56

Noninvasive Assessment of Tumor VEGF Receptors in Response to Treatment with Pazopanib: A Molecular Imaging Study[1]

Francis G. Blankenberg*, Zoia Levashova*, Susanta K. Sarkar†, John Pizzonia‡, Marina V. Backer§ and Joseph M. Backer§

*Department of Pediatrics & Division of Nuclear Medicine/Department of Radiology & MIPS (Molecular Imaging Program at Stanford) Stanford University, Stanford, CA 94304, USA; †Medicines Development, Oncology R&D, GlaxoSmithKline, Collegeville, PA 19426, USA; ‡FUJIFILM Medical Systems USA, Inc, Woodbridge, CT 06525, USA; §SibTech, Inc, Brookfield, CT 06804, USA

Abstract

Vascular endothelial growth factor (VEGF) and its receptors (VEGFRs) drive angiogenesis, and several VEGFR inhibitors are already approved for use as single agents or in combination with chemotherapy. Although there is a clear benefit with these drugs in a variety of tumors, the clinical response varies markedly among individuals. Therefore, there is a need for an efficient method to identify patients who are likely to respond to antiangiogenic therapy and to monitor its effects over time. We have recently developed a molecular imaging tracer for imaging VEGFRs known as scVEGF/^{99m}Tc; an engineered single-chain (sc) form of VEGF radiolabeled with technetium Tc 99m (^{99m}Tc). After intravenous injection, scVEGF/^{99m}Tc preferentially binds to and is internalized by VEGFRs expressed within tumor vasculature, providing information on prevalence of functionally active receptors. We now report that VEGFR imaging readily detects the effects of pazopanib, a small-molecule tyrosine kinase inhibitor under clinical development, which selectively targets VEGFR, PDGFR, and c-Kit in mice with HT29 tumor xenografts. Immunohistochemical analysis confirmed that the changes in VEGFR imaging reflect a dramatic pazopanib-induced decrease in the number of VEGFR-2$^+$/CD31$^+$ endothelial cells (ECs) within the tumor vasculature followed by a relative increase in the number of ECs at the tumor edges. We suggest that VEGFR imaging can be used for the identification of patients that are responding to VEGFR-targeted therapies and for guidance in rational design, dosing, and schedules for combination regimens of antiangiogenic treatment.

Translational Oncology (2010) 3, 56–64

Introduction

Vascular endothelial growth factor (VEGF) and its receptors (VEGFRs) provide the proangiogenic signaling that is required for growth and continued survival of endothelial cells (ECs) within the angiogenic vasculature of primary tumors and metastatic lesions. The critical role of VEGF/VEGFR signaling in the generation and maintenance of the tumor vasculature has led to massive efforts to develop drugs, such as antibodies against VEGF and VEGFRs, or small-molecule inhibitors of VEGFR tyrosine kinase, designed to selectively inhibit this pathway. Several antiangiogenic drugs are already approved for clinical use, either as monotherapy or as part of a combination therapy, and many clinical trials are in progress for approved and experimental inhibitors of the VEGF/VEGFR signaling pathway [1,2]. Unfortunately, the benefit to a large percentage of patients from these targeted drug treatments is still limited. This is most likely due to the current lack of optimal ways to evaluate a particular targeted drug; for example, how to identify which patient population would benefit most from that drug [3–7]. The mechanisms that determine sensitivity and resistance of ECs to antiangiogenic drugs are both complex and poorly understood [7]. There are several experimental models in which antiangiogenic drugs induce relatively rapid regression of tumor vascularization [8–13], underscoring the important relationship

Address all correspondence to: Joseph M. Backer, Ph.D., SibTech, Inc, 115A Commerce Dr, Brookfield, CT 06804. E-mail: jbacker@sibtech.com

[1]This study was supported by National Institutes of Health grants 2R44CA113080 and R43EB006679 to J.M.B. and by GlaxoSmithKline.

Received 9 September 2009; Revised 9 September 2009; Accepted 14 September 2009

1944-7124 DOI 10.1593/tlo.09271

between VEGF/VEGFR signaling and EC viability within a tumor [14]. However, in most experimental systems and, certainly, in patients, VEGF/VEGFR–directed drugs inhibit tumor growth, rather than lead to tumor regression, suggesting that a sufficient number of tumor ECs can survive and form functional blood vessels. Furthermore, it seems that decline in tumor vascularization might be transient and it is followed by an "adaptive revascularization," as defined by Bergers and Hanahan [7]. This phenomenon may be particularly important when antiangiogenesis treatment is interrupted [14–21]. The ability to measure the dynamics of these processes *in vivo* and their susceptibility to drug intervention may hold the key to successful clinical application of VEGF/VEGFR–directed therapies [5].

We have recently developed a family of tracers for assessing VEGFR expression with different imaging modalities [22,23]. These tracers are based on an engineered VEGFR ligand, a single-chain (sc) VEGF composed of two fused 3-112 amino acid (aa) fragments of VEGF121 and an N-terminal 15-aa Cys tag with a unique cysteine residue for site-specific conjugation of various payloads [22,24]. Direct radiolabeling of Cys tag in scVEGF with technetium Tc 99m (^{99m}Tc) yields a stable radiotracer scVEGF/^{99m}Tc for single photon emission computed tomography (SPECT) imaging, which rapidly binds to and is internalized by VEGF receptors, providing imaging information on the prevalence of VEGFR in tumor vasculature in various tumor models [23].

We report here that SPECT imaging of VEGFR with scVEGF/^{99m}Tc provides a highly sensitive approach to the analysis of the complex dynamics of VEGFR expression and activity during the treatment of HT29 xenografts with pazopanib, a small-molecule tyrosine kinase inhibitor (targeting VEGFR, PDGFR, and c-Kit) currently under clinical development [25,26]. Changes in tracer uptake seen at SPECT and autoradiography directly correlated with the immunohistochemical analyses of the EC markers VEGFR-2 and CD31 and suggest that scVEGF/^{99m}Tc imaging will be useful clinically for the assessment of the therapeutic efficacy of current and future antiangiogenic drugs.

Methods

Reagents

scVEGF and scVEGF/Cy (scVEGF site-specifically labeled with Cy5.5-maleimide) were prepared at SibTech, as described previously [22]. scVEGF/AlexaFluor594 was prepared at SibTech by site-specific conjugation of AlexaFluor594-maleimide (Invitrogen, Carlsbad, CA) to scVEGF, as described for synthesis scVEGF/Cy5.5 [22], followed by reverse phase high-performance liquid chromatography purification. Pazopanib [5-({4-[2,3-dimethyl-2*H*-indazole-6-yl) methylamino]2-pyrimidinyl}amino)-2methylbenzenesulfonamide] was synthesized at GlaxoSmithKline (Collegeville, PA). For tissue culture assays, pazopanib was obtained in a purified powder and reconstituted in DMSO at a concentration of 10 mM before use. For the tumor xenograft studies, pazopanib was formulated in aqueous 0.5% hydroxypropylmethylcellulose and 0.1% Tween 80.

Tissue Culture

HT29 cells were obtained from ATCC (HTB-38; Manassas, VA) and maintained in McCoy's 5A medium supplemented with 10% FBS (Gibco, Carlsbad, CA). PAE/KDR cells, porcine aortic ECs expressing full-length human VEGFR-2, and wild-type PAE cells (described in Backer et al. [22]) were maintained in Dulbecco's modified Eagle's medium high-glucose (Invitrogen) supplemented with 10% FBS (HyClone, Waltham, MA) and 2 mM L-glutamine.

In Vitro *Cellular Uptake of scVEGF-Based Tracer*

For quantitative uptake experiments, PAE/KDR and PAE cells were plated in black clear bottom 96-well plates (BD Falcon, Franklin Lakes, NJ) at 20,000 cells per well. Twenty hours later, cells were shifted to fresh culture medium either with or without 1 μM pazopanib and incubated for 1 hour in CO_2 incubator. scVEGF/Cy was titrated in culture medium with or without 1 μM pazopanib, then added to cells in corresponding triplicate wells, and incubated for 20 minutes under normal tissue culture conditions. Then media were removed, cells were washed extensively with PBS, then with PBS containing 0.5 M NaCl, fixed in fresh 4% ultrapure methanol-free formaldehyde (Polysciences, Warrington, PA), air-dried, and tracer uptake was quantitated by imaging plates in Starion FLA-9000 imager (FUJIFILM Medical Systems USA, Woodbridge, CT). For microscopy, PAE/KDR cells were plated on four-well chamber slides (Nunc, Rochester, NY), 50,000 cells per well, incubated for 1 hour with or without 10 μM pazopanib, and then for 20 minutes with 5 nM scVEGF/AlexaFluor594, with or without 10 μM pazopanib. After extensive washing, cells were mounted in Vectashield with 4′,6-diamidino-2-phenylindole (Vector Labs, Burlingame, CA) and observed under an AxioObserver Zeiss microscope (Carl Zeiss MicroImaging, Inc, Thornwood, NY).

Mice

Protocol for the animal studies was approved by the Institutional Animal Care and Use Committees at Stanford University. Five- to six-week-old female Swiss nude mice (NSWNU-M-F; Taconic, Hudson, NY) received HT29 (1.5-1.8 × 10^6 cells per mouse) subcutaneously in the left flank regions. Pazopanib was given as gavage, twice daily at 100 mg/kg, for a total dosage of 200 mg/kg daily. At the end of the study, tumors were harvested, flash-frozen, and cryosectioned to obtain 60-μm, 20-μm, and 7-μm sections.

Immunohistochemistry

Fluorescent immunostaining of 7-μm tumor cryosections for VEGFR-2(KDR/Flk-1), CD31(PECAM), and VEGFR-1(Flt-1) was done as described [22]. Slides were observed and digitized on an AxioObserver Zeiss microscope using 43× oil and 5× objectives. Chromogenic immunostaining of 20-μm cryosections for VEGFR2 and for CD31 was developed with VECTASTATIN Elite ABC Kit and VIP Substrate Purple Kit (Vector Labs).

SPECT Imaging

scVEGF was radiolabeled with ^{99m}Tc to an activity of 200 μCi/μg protein as described [23]. In all imaging experiments, a dose of 2 to 4 mCi of scVEGF/^{99m}Tc was injected into the retro-orbital venous sinus in a volume of 100 to 220 μl (10-20 μg protein) followed by imaging 2 hours later. Briefly, images taken with the following parameters: 64 steps, 360° rotation, 30 seconds per step, 2.7 cm field of view, 0.5 mm pinhole collimator, 64 × 64 imaging matrix. Image reconstruction and analyses were performed with standard Mirage (Siemens, Malvern, PA) image processing software using OSEM reconstruction (20 iterations, 8 subsets), and no filter. Tumor uptake analysis of SPECT imaging data was performed using parametric three-dimensional regions of interest, interactively placed and sized, as described elsewhere [30]. Regions of interest of a standard dose in a

capillary tube and the whole of each tumor were drawn, and histogram for counts *versus* number of voxels was obtained. Maximal tumor uptake per voxel for each tumor was then defined as 100 counts (cts) per voxel and recalculated values of cts per voxel were tabulated together with percentile of corresponding voxels, defined as 100 × (number of voxel with given cpm) / (total number of voxels). The average counts/voxel for the upper 98th percentile of voxels were calculated from the histograms of the whole of each tumor, and the counts/voxel at 50th percentile were subtracted to correct for background activity. The resulting average values of the upper 98th percentile of voxels (U-98th%) was then used for comparison of uptake in the high uptake areas for all tumors.

Soluble VEGFRs

Blood was collected from deeply anesthetized mice by cardiac puncture through 21-G needle into 1-ml syringes containing 3.8% Na citrate, pH 7.0. Collected blood was transferred into preweighed microcentrifuge tubes, weighed to calculate the size of blood sample, incubated on ice for 30 minutes, and centrifuged at 4000*g* for 5 minutes at 4°C. Clarified plasma was carefully collected, immediately frozen, and stored at −80°C until testing. Concentrations of soluble VEGFR-1 and VEGFR-2 in murine plasma were determined by ELISA using Quantikine kits from R&D Systems (Minneapolis, MN). Standard calibration curve for each receptor was generated during the assay. All samples were tested in duplicates. Because the levels of sVEGFR-1 varied within an order of magnitude, we validated the sensitivity of the kit with control soluble mouse VEGFR-1 and found it to be corresponding to the manufacturer's specifications (714 pg/ml of control VEGFR-1, which is within expected range of 503-838 pg/ml). We therefore assumed that the lower level of VEGFR-1 in HT-29–bearing Swiss mice might be a model-specific characteristic.

Results

Pazopanib Does Not Inhibit VEGFR-2–Mediated Internalization of scVEGF-Based Tracers

Because imaging with scVEGF/^{99m}Tc requires VEGFR-mediated internalization of the tracer, and pazopanib inhibits VEGFR tyrosine kinase activity, it was important to establish if tyrosine phosphorylation is required for internalization of scVEGF-based tracers. Studies of mutant VEGFR-2 have indicated that tyrosine phosphorylation is required for efficient internalization [27,28], whereas experiments with a tyrosine phosphorylation inhibitor SU5416 demonstrated that only intracellular processing of the receptors, but not their internalization, is phosphorylation-dependent [29]. In view of these somewhat conflicting results, we explored whether pazopanib can affect internalization of scVEGF-based fluorescent tracers in porcine aortic ECs PAE/KDR. As we reported previously [22], PAE/KDR cells, but not parental PAE cells without VEGFR-2, rapidly internalize scVEGF/Cy, indicating VEGFR-2–mediated tracer uptake. Pazopanib inhibits human VEGFR-2 with a half maximal inhibitory concentration of 30 ± 13 nM [25]. We found that at a concentration of 10 nM, it efficiently blocked scVEGF-induced VEGFR-2 tyrosine phosphorylation in PAE/KDR cells engineered to express 100,000 human VEGFR-2 per cell (Figure 1*A*). However, the dose-dependent intracellular accumulation of scVEGF/Cy fluorescent tracer by these cells was not affected in the presence of pazopanib, even after 1 hour before incubating with as high as 1 μM of the inhibitor (Figure 1*B*). Fluorescent microscopy with scVEGF/AlexaFluor594 tracer also indicated similar internalization of the tracer in pazopanib-treated and control PAE/KDR cells (Figure 1*C*). Taken together, these results suggest that it is unlikely that pazopanib would inhibit VEGFR-mediated internalization of scVEGF/^{99m}Tc tracer *in vivo*.

SPECT Imaging of Pazopanib-Induced VEGFR Changes

For imaging studies, we used subcutaneous human colon cancer HT29 tumors grown in Swiss nude mice, a model that has been reported to be highly sensitive to treatment with pazopanib [25]. After tumors were grown for 19 to 20 days, mice (n = 10) underwent SPECT imaging with scVEGF/^{99m}Tc (day 0) and were then separated into control and pazopanib-treated groups and reimaged at days 5 and 15. As shown in Figure 2*A* for a representative control mouse, in serial SPECT imaging on days 0, 5, and 15, we observed a selective tracer uptake in the tumor area, with preferential accumulation of the tracer at the edges of the tumor in the so-called angiogenic rim (Figure 2*A*). In contrast, as shown in Figure 2*A* for a representative pazopanib-treated mouse, there was a marked decrease in the tracer uptake in tumor area on day 5 relative to day 0. This decrease was followed by a resurgence of the tracer uptake on day 15 relative to day 5 (Figure 2*A*).

To characterize temporal changes in tracer uptake at the tumor edges, a quantitative histogram analysis of each SPECT image was performed as described elsewhere [30]. The average value of focal activity expressed as counts/voxel was determined for the upper 98th percentile of voxels (U-98th%) within a tumor. We found that, despite tumor growth, the average U-98th% uptake values were not statistically different from one another at day 0, 5, or 15 in control mice undergoing serial SPECT imaging (Figure 2*B*). In contrast, in pazopanib-treated mice, the average U-98th% uptake values decreased three-fold (n = 4, P = .001) at day 5 relative to day 0 and 1.5-fold (n = 3, P = .05) at day 15 relative day 0 (Figure 2*B*). The 1.8-fold increase (n = 3, P = .004) in the average U-98th% uptake values from day 5 to day 15 reflected the relative resurgence of tracer uptake observed by SPECT imaging (Figure 2*A*).

Importantly, a three-fold decrease in the average U-98th% uptake values after 5 days of pazopanib treatment was observed when the difference in tumor weight in treated *versus* control mice was only 25% (P = .016) (Figure 2*C*). However, relative resurgence in tracer uptake after 15 days of pazopanib treatment was observed despite continuous inhibition of tumor growth leading to an approximately two-fold smaller tumor weight of treated *versus* control mice (P = .0001). Thus, SPECT imaging with scVEGF/^{99m}Tc can detect pazopanib-induced changes in tumor vasculature well before they affect tumor growth and morphology.

Pazopanib-Induced Changes in scVEGF/^{99m}Tc Tracer Uptake, as Seen by Autoradiography

To further characterize the effects of pazopanib on tracer uptake, we compared autoradiographs of serial tumor sections obtained from additional groups of 5- and 15-day treated and time-matching control scVEGF/^{99m}Tc-injected mice. As shown in Figure 3, *A* and *B*, preferential accumulation of radioactivity at the tumor edges was readily detected on autoradiographs of serial sections from control mice. As shown in Figure 3*C*, a 5-day pazopanib treatment resulted in a markedly lower tumor edge tracer uptake in treated *versus* control mice (compare Figure 3*C* and Figure 3*A*). However, as shown in Figure 3*D*, a 15-day

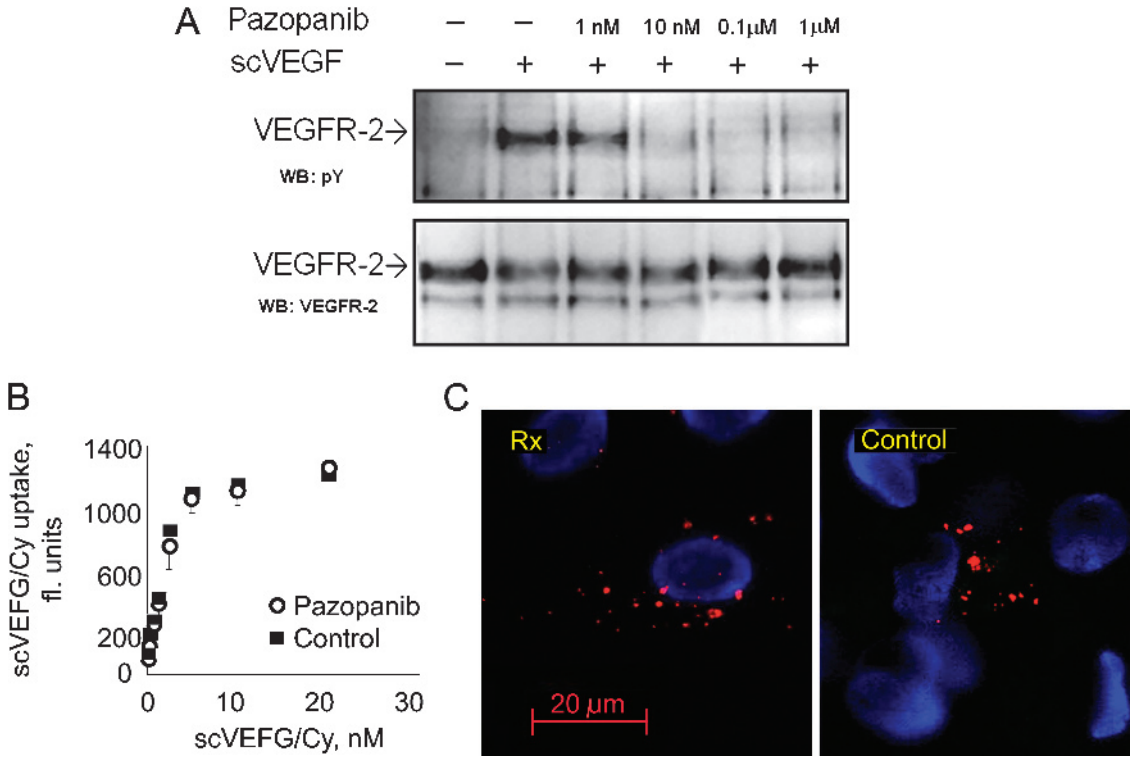

Figure 1. Pazopanib does not block VEGFR-2–mediated uptake of scVEGF-based fluorescent tracers. (A) Pazopanib blocks scVEGF-induced VEGFR-2 tyrosine phosphorylation in PAE/KDR cells expressing 100,000 VEGFR-2 per cell. Cells were plated on 24-well plates, 75,000 cells per well, in complete culture medium, and shifted to serum-free medium 6 hours later. Top panel: After overnight serum starvation, cells were incubated for 10 minutes at 37°C with 10 nM scVEGF, either alone or in the presence of pazopanib, then lysed and analyzed by Western blot analysis with phosphotyrosine-specific antibody (pY, clone PT-66; Sigma, St. Louis, MO). Bottom panel: To ensure equal protein loading, the blot was stripped and reprobed with VEGFR-2–specific rabbit antiserum as described [22]. (B) Pazopanib does not inhibit dose-dependent uptake of scVEGF/Cy by PAE/KDR cells. A 20-minute tracer uptake by PAE/KDR (~10^5 VEGFR-2/cell) and PAE (no VEGFR-2) cells in the presence or absence of 1 μM pazopanib (after 1 hour before incubation) was quantitated in triplicate wells using Starion FLA-9000 imager (FUJIFILM Medical Systems USA). (C) Pazopanib does not inhibit uptake of scVEGF/AlexaFluor594 fluorescent tracer by PAE/KDR cells. A 20-minute tracer uptake by PAE/KDR cells in the presence or absence of 10 μM pazopanib was visualized with an AxioObserver Zeiss microscope, using 43× oil objective. *Control*, untreated cells; *Rx*, pazopanib-treated cells.

pazopanib treatment resulted in a relative resurgence of tumor edge uptake, when compared with a 5-day group (compare Figure 3*D* and Figure 3*C*). In fact, as judged by autoradiography, some sections from 15-day treated mice demonstrated a level of tumor edge tracer uptake comparable to that in time-matching control mice (compare Figure 3*D* and Figure 3*B*). Thus, autoradiography analysis supported SPECT imaging finding of decrease and relative resurgence of scVEGF/^{99m}Tc tracer uptake in the course of pazopanib treatment.

Immunohistochemical Analysis of Pazopanib-Induced VEGFR Changes

The uptake of scVEGF/^{99m}Tc by VEGFR-expressing cells depends on several parameters, such as the number of VEGFR sites per cell, the number of VEGFR-overexpressing cells, efficacy of scVEGF/^{99m}Tc–VEGFR complex internalization, and VEGFR recycling. Furthermore, spatial distribution of those parameters defines the heterogeneity in tracer uptake, including prominent uptake at the tumor edges. To assess VEGFR distribution, tumors from control and treated mice were cryosectioned for immunohistochemical analysis of VEGF receptors, VEGFR-1 and VEGFR-2, as well as pan-endothelial marker CD31 (PECAM) that unambiguously identifies ECs. Double-fluorescent immunostaining established that, in HT29 tumors, VEGFR-1 was not expressed on CD31-positive ECs (Figure 4*A*). In contrast, VEGFR-2 was expressed exclusively on CD31-positive ECs (Figure 4*B*). The density of CD31$^+$/VEGFR-2$^+$ cells was 2- to 2.5-fold higher in the vascularized areas at the tumor edges relative to tumor center (Figure 4*C*, compared with Figure 4*B*).

Pazopanib treatment strongly affected both VEGFR-2 and CD31 immunostaining of tumor edge areas with distinctively different results observed in 5- and 15-day regimen groups. A 5-day regimen resulted in a rather dramatic decrease in VEGFR-2 and CD31 immunostaining relative to control (Figure 4*D*), but there was a visible resurgence in VEGFR-2 and CD31 immunostaining reflecting revascularization at the tumor edges, which was particularly prominent at the low-magnification images (Figure 4*E*). Furthermore, in the 15-day treatment group, CD31 and VEGFR-2 immunostaining at the edges of the tumor sections was about as prominent as for the time cohorts of control mice. In contrast, pazopanib treatment did not change VEGFR-1 immunostaining (Figure 4*F*).

Unlike dynamic vascular remodeling at the tumor edges, the decrease in VEGFR-2 and CD31 immunostaining in the tumor center areas detected at the 5-day group (Figure 5*A*) persisted after 15 days of pazopanib treatment (Figure 5*B*). Quantitative analysis of immunostaining for CD31 and VEGFR-2 in central areas in high-magnification fields (n = 5) confirmed a dramatic difference in marker staining in treated groups for both treatment regimens (Figure 5*C*).

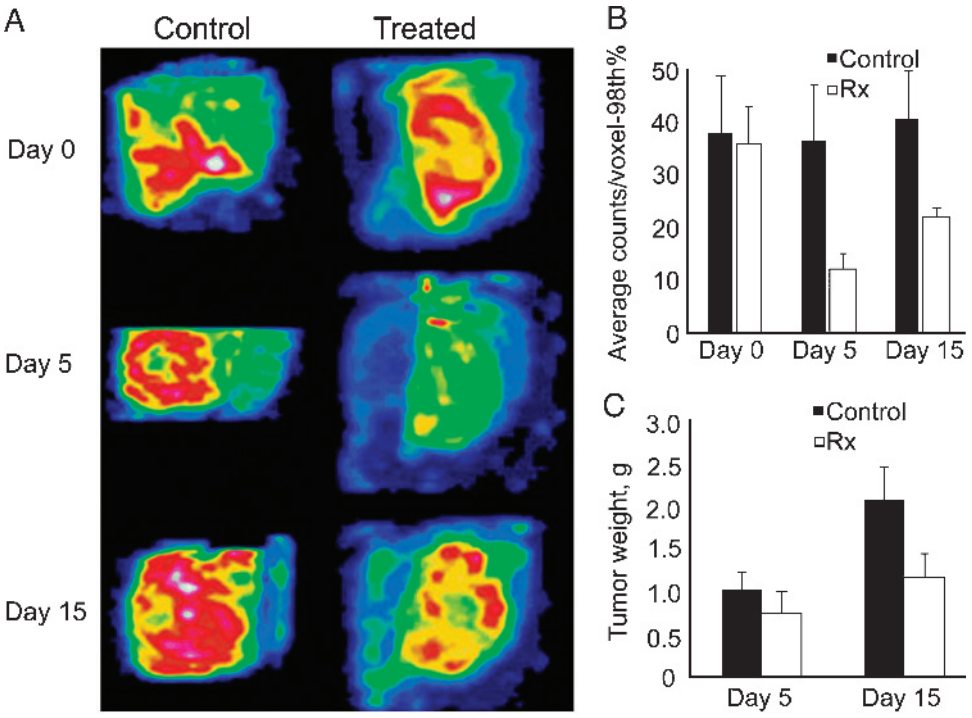

Figure 2. Pazopanib treatment affects scVEGF/^{99m}Tc tracer uptake. (A) Representative anterior oblique views of the tumors from control and treated mice reconstructed from three-dimensional data sets obtained in serial SPECT imaging. (B) Pazopanib significantly affects tracer uptake in areas of maximal activity. The average activity of the upper 98th percentile of voxels (U-98th%) was calculated from the longitudinal SPECT imaging for each mouse on days 0, 5, and 15 for treated and time cohorts of control mice. (C) Tumor weights for control and treated mice. *Control*, untreated mice; *Rx*, pazopanib-treated mice.

Taken together, immunostaining analysis suggests that the decrease in scVEGF/^{99m}Tc uptake on day 5 is due to pazopanib-induced decrease in the number of CD31$^+$/VEGFR-2$^+$ tumor ECs throughout the tumor, including tumor edges. Conversely, a subsequent resurgence in scVEGF/^{99m}Tc uptake at the tumor edges on day 15 is supported by the resurgence of CD31$^+$ and VEGFR-2$^+$ ECs in the same areas. It remains to be established if enhanced VEGFR-2 internalization and/or receptor recycling in proliferating ECs also contribute to enhanced tracer uptake.

Effect of Pazopanib on Circulating Soluble VEGFR-2 and VEGFR-1 Receptors

Extracellular fragments of VEGFR-1 and VEGFR-2, so-called soluble VEGF receptors (sVEGFRs), are present in blood. Thus, one could assume that pazopanib treatment increases the level of soluble receptors, which then sequester scVEGF/^{99m}Tc tracer, leading to decreased uptake in tumor vasculature. To test this assumption, we measured the levels of sVEGFR-1 and sVEGFR-2 in plasma of control and treated mice using sensitive quantitative ELISA. The levels of soluble VEGFR-2 in control

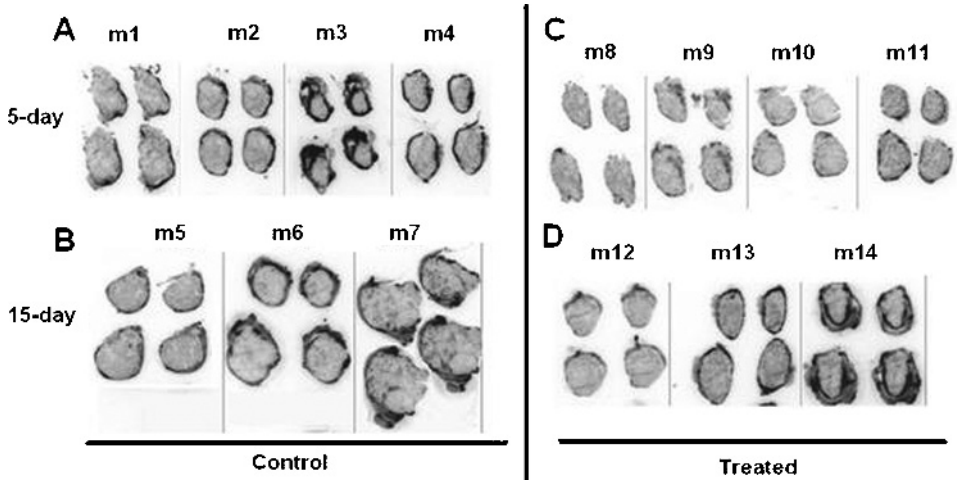

Figure 3. Decrease and resurgence of scVEGF/^{99m}Tc uptake in the course of pazopanib treatment. Autoradiographs of serial 60-μm sections from individual tumors harvested from treated and control and treated mice after 5- (A, C) and 15-day (B, D) treatment regimens.

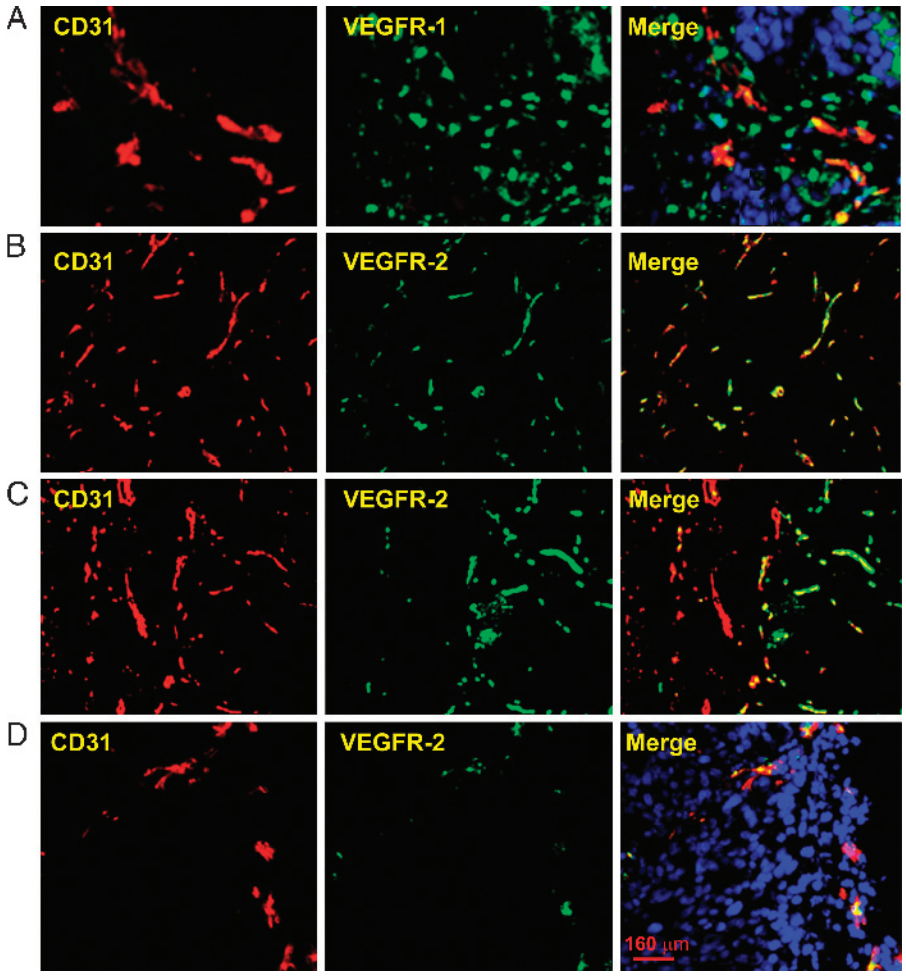

Figure 4. Effects of pazopanib treatment on immunostaining for VEGFR-1, VEGFR-2, and CD31. (A–D) Images of representative microscopy fields (objective, ×5) with fluorescent double immunostaining for indicated markers and merged images with counterstaining for nuclei at panels A and D. (A) Control tumor. (B) Control tumor, representative field from the tumor interior. (C) Control tumor, representative field from the tumor edge with higher density of markers. (D) Five-day pazopanib-treated tumor. Tumor edge on the right is visible on the merged panel. (E) Images of representative fields with chromogenic staining for CD31 and VEGFR-2 obtained from three individual mice after a 15-day pazopanib treatment and three time-matched control mice; objective, ×4. (F) Pazopanib treatment does not affect VEGFR-1. Images of representative fields with immunostaining for VEGFR-1 (green) and counterstaining for nuclei (blue) from control and pazopanib-treated mice. Bar, 20 μm.

and treated mice varied from 20 to 69 ng/ml, which is within the reported range for murine plasma (27-96 ng/ml). No significant changes in soluble VEGFR-2 in treated *versus* control mice were detected for 5- and 15-day treatment groups (Figure 6*A*). The levels of soluble VEGFR-1 varied within one order of magnitude, from 220 to 2220 pg/ml, and seemed to be below the expected range of soluble VEGFR-1 in murine plasma (2750-8026 pg/ml). However, no significant changes in sVEGFR-1 in treated *versus* control mice were detected for 5- and 15-day treatment groups (Figure 6*B*).

Discussion

Variable responses of individual patients to cancer therapy have stimulated the development of noninvasive imaging methods that can detect early treatment response [31,32]. A recent report demonstrated that changes in [^{18}F] 2-fluoro-2-deoxy-D-glucose (FDG) positron emission tomography (PET) tracer uptake can detect response to chemotherapy as early as 24 hours after the onset of treatment [33]. Currently, downstream effects of VEGFR-directed therapy are imaged in clinic by computed tomography and dynamic contrast-enhanced magnetic resonance imaging. Several clinical trials are in progress to determine the utility of PET imaging of tumor metabolism with ^{18}F-FDG and ^{18}F-FLT, and $\alpha_v\beta_3$ integrins with ^{18}F-RGD-peptide based tracers (www.clinicaltrials.gov). However, as important as downstream markers are, molecular imaging of the drug target itself provides critical information on the target prevalence, opening opportunities for treatment management and optimization. This is particularly true for the development of antiangiogenic therapies, where the lack of suitable noninvasive methods for monitoring the drug's target is the critical barrier in the evaluation of new antiangiogenic therapies [5].

We report here that the intricate temporal dynamics of VEGFR-2 response to pazopanib treatment can be readily measured with scVEGF/^{99m}Tc by SPECT imaging. Our SPECT and autoradiography data indicate that in the HT29 tumor model, pazopanib induces a very rapid decrease in tracer uptake even before pazopanib-induced changes in tumor size. As judged by immunohistochemical analyses of VEGFR-2 and pan-endothelial CD31 markers, the decrease in tracer uptake coincides with a remarkable depletion of CD31$^+$/VEGFR-2$^+$ ECs in tumor vasculature. A similar rapid regression of tumor vasculature in other murine tumor

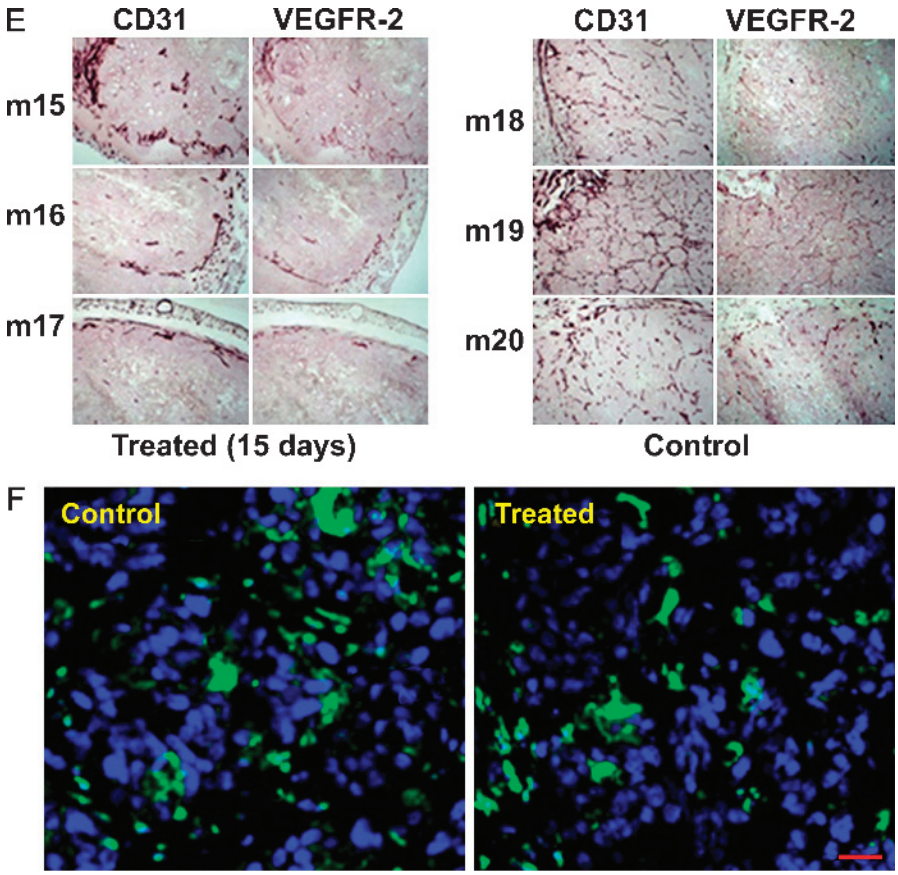

Figure 4. (*continued*).

xenograft models has also been reported for other VEGFR-2 tyrosine kinase inhibitors, such as sorafenib [10], sunitinib [11], and AZD2171 [12]. However, as treatment continues, scVEGF/^{99m}Tc uptake increases, as judged by both SPECT imaging and autoradiography. Correspondingly, immunohistochemical analyses indicate reestablishment of CD31$^+$/VEGFR-2$^+$ ECs at the tumor edges. It should be noted that immunohistochemical evidence of the overall tumor revascularization either after antiangiogenic drug withdrawal [15,16,20,21] or after long treatment with anti–VEGFR-2 antibody [34] has been reported. However, our imaging results seem to suggest a rather rapid and localized reestablishment of CD31$^+$/VEGFR-2$^+$ ECs at the tumor edges only. Taken together, our data indicate that scVEGF/^{99m}Tc SPECT imaging faithfully reflects the temporal and spatioselective response of VEGF receptors to pazopanib treatment.

Currently, there is an intense interest in the mechanisms of actions of drugs that target VEGF/VEGFR signaling, as well as in the mechanisms responsible for resistance to such drugs, named adaptive/evasive resistance, which lead to vascular resurgence [7,35]. The appearance of highly vascularized areas at the tumor edges supports a continuous tumor growth and even supports metastatic dissemination [20,21,36]. It is expected that revascularization would play a critical role in response to drugs targeting VEGF/VEGFR signaling not only in mouse models but also in cancer patients [37].

Conversely, revascularization might provide for better delivery of chemotherapeutic drugs to tumor growth areas, justifying the combination regimens and particularly metronomic combinations [38,39]. We are currently extending our imaging studies to establish the patterns of VEGFR changes in various multidrug treatment regimens.

To the best of our knowledge, we present here the first direct real-time evaluation of the complex dynamics of VEGFR expression in response to a VEGFR-targeted therapy. In principle, imaging with scVEGF-based tracers can be extended to human use providing for new opportunities in evidence-based treatment management of VEGFR-targeted therapies including patient selection, dose optimization, and rational design of combination regimens. For example, scVEGF/^{99m}Tc tracer uptake at the early stages of treatment might define the preexisting drug target levels and characterize the drug target depletion. Nevertheless, resurgence of scVEGF/^{99m}Tc tracer uptake might suggest a better timing for combination or metronomic therapy and/or emerging resistance to VEGF/VEGFR inhibitors throughout the course of treatment.

What are the foreseeable barriers in the translation of VEGFR imaging with scVEGF/^{99m}Tc into clinic? First, there are indications that SPECT imaging might be less advantageous than PET imaging with respect to spatial resolution and possibly contrast-to-noise ratios [40]. From this prospective, it might be more beneficial to develop tracers based on scVEGF–polyethylene glycol–DOTA conjugate [22] that can be radiolabeled with ^{99m}Tc for SPECT, ^{64}Cu and ^{68}Ga for PET imaging, as well as with therapeutic radionuclides. Second, scVEGF-based tracers might be incompatible with one of the most widely used VEGF/VEGFR–directed drugs, anti-VEGF antibody bevacizumab (Avastin). Fortunately, it was reported that a single G88A substitution in human VEGF eliminates Avastin binding without affecting VEGF affinity to VEGFR [41]. Thus, if necessary, minor reengineering of scVEGF would make scVEGF-based tracers suitable for monitoring treatments with bevacizumab. Third, there are legitimate concerns associated with short-

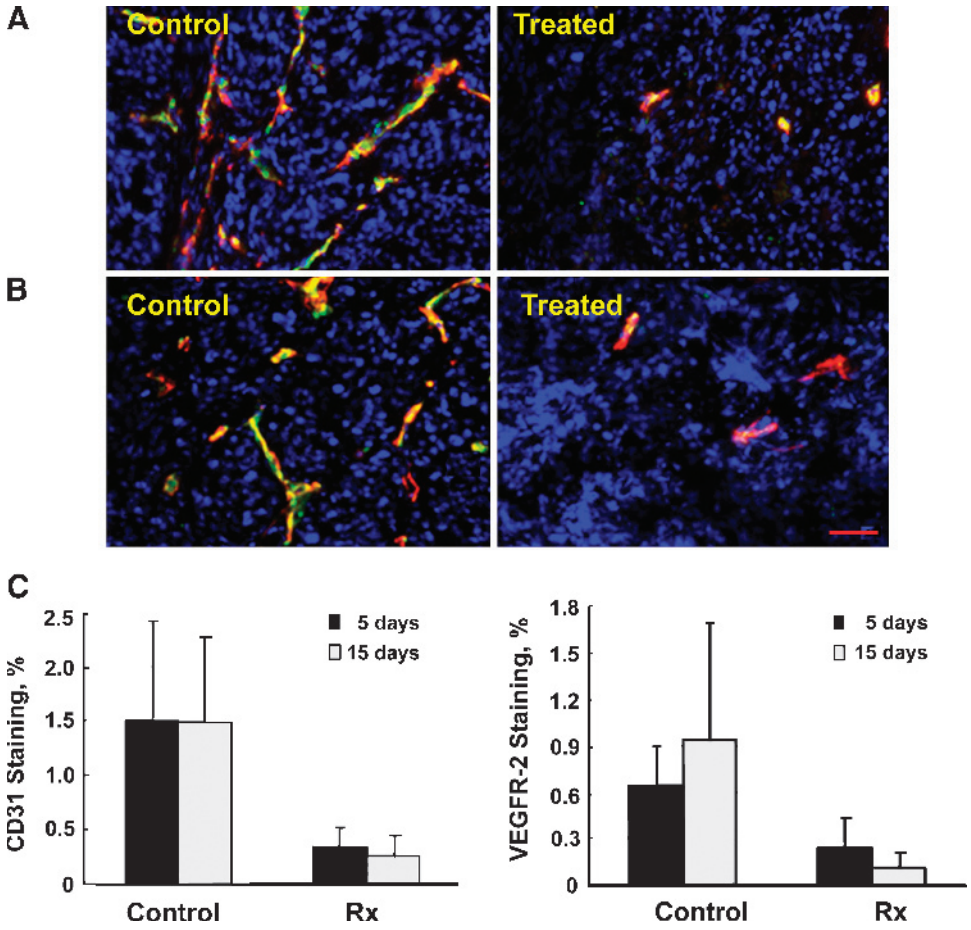

Figure 5. Pazopanib treatment induced a dramatic decrease in CD31 and VEGFR-2 immunohistochemical staining in intratumoral vasculature. (A, B) Representative high-magnification (40× oil) microscopy field with double-fluorescent immunostaining for CD31 (red) and VEGFR-2 (green) of the tumor center area. Bar, 20 μm. (A) Five-day pazopanib treatment and time-matching control; (B) 15-day pazopanib treatment and time-matching control. (C) Quantitative analysis of immunostaining for CD31 and VEGFR-2 in high-magnification fields ($n = 5$). Counterstaining for nuclei with DAPI (blue). *Control*, untreated mice; *Rx*, pazopanib-treated mice.

and long-term physiological effects of scVEGF-based tracers. Although only detailed safety studies with can address these concerns, past clinical trials suggest that several infusions of recombinant VEGF165 at 0.05 μg/kg per minute for 20 minutes are well tolerated [42]. Assuming the same safety profile for scVEGF-based tracers, this dosage would be more than sufficient for injection of ~10 mCi of tracer with a readily achievable specific activity of ~200 μCi/μg. Taken together; these considerations suggest that technical barriers for using scVEGF/^{99m}Tc can be overcome. Although only clinical trials can establish clinical relevance and predictive value of any biomarker [43], we expect that VEGFR imaging will be useful for surveillance and evaluation of responses to VEGF/VEGFR–directed therapies.

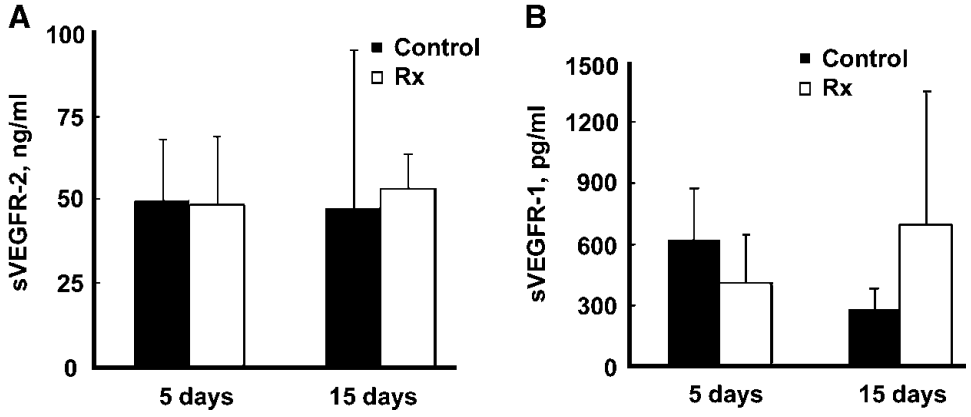

Figure 6. Pazopanib does not induce statistically significant changes in the levels of soluble VEGF receptors. sVEGFR-2 (A) and sVEGFR-1 (B) in plasma of HT29 tumor-bearing mice. *Control*, untreated mice; *Rx*, pazopanib-treated mice.

Acknowledgments

The authors thank H. Ball, R. Kumar, and L. Pandite for helpful discussions and D. Roychowdhury for critical reading of the manuscript and constant encouragement and support.

References

[1] Jubb AM, Oates AJ, Holden S, and Koeppen H (2006). Predicting benefit from antiangiogenic agents in malignancy. *Nat Rev Cancer* **6**, 626–635.

[2] Hayden EC (2009). Cutting off cancer's supply lines. *Nature* **458**, 686–687.

[3] Lin MI and Sessa WC (2004). Antiangiogenic therapy: creating a unique "window" of opportunity. *Cancer Cell* **6**, 529–531.

[4] Jain RK, Duda DG, Clark JW, and Loeffler JS (2006). Lessons from phase III clinical trials on anti-VEGF therapy for cancer. *Nat Clin Pract Oncol* **1**, 24–40.

[5] Sessa C, Guiba A, Del Conte G, and Ruegg C (2008). Biomarkers of angiogenesis for the development of antiangiogenic therapies in oncology: tools or decorations? *Nat Clin Pract Oncol* **5**, 78–91.

[6] Ellis LM and Hicklin DJ (2008). VEGF-targeted therapy: mechanisms of anti-tumour activity. *Nat Rev Cancer* **8**, 579–591.

[7] Bergers G and Hanahan D (2008). Modes of resistance to antiangiogenic therapy. *Nat Rev Cancer* **8**, 592–603.

[8] Franco M, Man S, Chen LL, Emmenegger U, Shaked Y, Cheung AM, Brown AS, Hicklin DJ, Foster FS, and Kerbel RS (2006). Targeted anti–vascular endothelial growth factor receptor-2 therapy leads to short-term and long-term impairment of vascular function and increase in tumor hypoxia. *Cancer Res* **66**, 3639–3648.

[9] Smith NR, James NH, Oakley I, Wainwright A, Copley C, Kendrew J, Womersley LM, Jurgensmeier JM, Wedge SR, and Barry ST (2007). Acute pharmacodynamic and antivascular effects of the vascular endothelial growth factor signaling inhibitor AZD2171 in Calu-6 human lung tumor xenografts. *Mol Cancer Ther* **6**, 2198–2208.

[10] Chang YS, Adnane J, Trail PA, Levy J, Henderson A, Xue D, Bortolon E, Ichetovkin M, Chen C, McNabola A, et al. (2007). Sorafenib (BAY 43-9006) inhibits tumor growth and vascularization and induces tumor apoptosis and hypoxia in RCC xenograft models. *Cancer Chemother Pharm* **59**, 561–574.

[11] Palmowski M, Huppert J, Hauff P, Reinhardt M, Schreiner K, Socher MA, Hallscheidt P, Kauffmann GW, Semmler W, and Kiessling F (2008). Vessel fractions in tumor xenografts depicted by flow- or contrast-sensitive three-dimensional high-frequency Doppler ultrasound respond differently to antiangiogenic treatment. *Cancer Res* **68**, 7042–7049.

[12] Bozec A, Gros FX, Penault-Llorca F, Formento P, Cayre A, Dental C, Etienne-Grimaldi MC, Fischel GL, and Milano G (2008). Vertical VEGF targeting: a combination of ligand blockade with receptor tyrosine kinase inhibition. *Eur J Cancer* **44**, 1922–1930.

[13] Selvakumaran M, Yao KS, Feldman MD, and O'Dwyer PJ (2008). Antitumor effect of the angiogenesis inhibitor bevacizumab is dependent on susceptibility of tumors to hypoxia-induced apoptosis. *Biochem Pharm* **75**, 627–638.

[14] Gerber HP, McMurtrey A, Kowalski J, Yan M, Keyt BA, Dixit V, and Ferrara N (1998). Vascular endothelial growth factor regulates endothelial cell survival through the phosphatidylinositol 3′-kinase/Akt signal transduction pathway. Requirement for Flk-1/KDR activation. *J Biol Chem* **273**, 30336–30343.

[15] Mancuso MR, Davis R, Norberg SM, O'Brien S, Sennino B, Nakahara T, Yao VJ, Inai T, Brooks P, Freimark B, et al. (2006). Rapid vascular regrowth in tumors after reversal of VEGF inhibition. *J Clin Invest* **116**, 2610–2621.

[16] Shaked Y, Ciarrocchi A, Franco M, Lee CR, Man S, Cheung AM, Hicklin DJ, Chaplin D, Foster FS, Benezra R, et al. (2006). Therapy-induced acute recruitment of circulating endothelial progenitor cells to tumors. *Science* **313**, 1785–1787.

[17] Shaked Y and Kerbel RS (2007). Antiangiogenic strategies on defense: on the possibility of blocking rebounds by the tumor vasculature after chemotherapy. *Cancer Res* **67**, 7055–7058.

[18] Burstein HJ, Elias D, Rugo HS, Cobleigh MA, Wolff AC, Eisenberg PD, Lehman M, Adams BJ, Bello CL, DePrimo SE, et al. (2008). Phase II study of sunitinib malate, an oral multitargeted tyrosine kinase inhibitor, in patients with metastatic breast cancer previously treated with an anthracycline and a taxane. *J Clin Oncol* **26**, 1810–1816.

[19] Johannsen M, Florcken A, and Bex A (2009). Can tyrosine kinase inhibitors be discontinued in patients with metastatic renal cell carcinoma and a complete response to treatment? A multicentre, retrospective analysis. *Eur Urol* **55**, 1430–1439.

[20] Ebos JM, Lee CR, Cruz-Munoz W, Bjarnason GA, Christensen JG, and Kerbel RS (2009). Accelerated metastasis after short-term treatment with a potent inhibitor of tumor angiogenesis. *Cancer Cell* **15**, 232–239.

[21] Paez-Ribes M, Allen E, Hudock J, Takeda T, Okuyama H, Vinals F, Inoue M, Bergers G, Hanahan D, and Casanovas DO (2009). Antiangiogenic therapy elicits malignant progression of tumors to increased local invasion and distant metastasis. *Cancer Cell* **15**, 220–231.

[22] Backer MV, Levashova Z, Patel V, Jehning BJ, Claffey K, Blankenberg FG, and Backer JM (2007). Molecular imaging of VEGF receptors in angiogenic vasculature with single-chain VEGF based probes. *Nat Med* **13**, 504–509.

[23] Levashova Z, Backer M, Backer JM, and Blankenberg FG (2008). Direct labeling of Cys-tag in scVEGF with technetium 99m. *Bioconjug Chem* **19**, 1049–1054.

[24] Backer MV, Levashova Z, Levenson R, Blankenberg FG, and Backer JM (2008). Cysteine-containing fusion tag for site-specific conjugation of therapeutic and imaging agents to targeting proteins. *Methods Mol Biol* **494**, 275–294.

[25] Kumar R, Knick VB, Rudolph SK, Johnson JH, Crosby RM, Crouthamel MC, Hopper TM, Miller CG, Harrington LE, Onori JA, et al. (2007). Pharmacokinetic-pharmacodynamic correlation from mouse to human with pazopanib, a multikinase angiogenesis inhibitor with potent antitumor and antiangiogenic activity. *Mol Cancer Ther* **6**, 2012–2021.

[26] Sloan B and Scheinfeld NS (2008). Pazopnib, a VEGF receptor tyrosine kinase inhibitor for cancer therapy. *Curr Opin Invest Drugs* **9**, 1324–1335.

[27] Dougher M and Terman BI (1999). Autophosphorylation of KDR in the kinase domain is required for maximal VEGF-stimulated kinase activity and receptor internalization. *Oncogene* **18**, 1619–1627.

[28] Santos SC, Miguel C, Domingues I, Calado A, Zhu Z, Wu Y, and Dias S (2007). VEGF and VEGFR-2 (KDR) internalization is required for endothelial recovery during wound healing. *Exp Cell Res* **313**, 1561–1574.

[29] Ewan LC, Jopling HM, Jia H, Mittar S, Bagherzadeh A, Howell GJ, Walker JH, Zachary IC, and Ponnambalam C (2006). Intrinsic tyrosine kinase activity is required for vascular endothelial growth factor receptor 2 ubiquitination, sorting and degradation in endothelial cells. *Traffic* **7**, 1270–1282.

[30] Tang XN, Wang Q, Koike MA, Cheng D, Goris ML, Blankenberg FG, and Yenari MA (2007). Monitoring the protective effects of minocycline treatment with radiolabeled annexin V in an experimental model of focal cerebral ischemia. *J Nucl Med* **48**, 1822–1828.

[31] Brindle K (2008). New approaches for imaging tumour responses to treatment. *Nat Rev Cancer* **8**, 1–14.

[32] Cho HJ, Ackerstaff E, Carlin S, Lupu ME, Wang Y, Rizwan A, O'Donoghue J, Ling CC, Humm JL, Zanzonico PB, et al. (2009). Noninvasive multimodality imaging of the tumor microenvironment: registered dynamic MRI and PET studies of a preclinical tumor model of tumor hypoxia. *Neoplasia* **11** (3), 247–259.

[33] Witney TH, Kettunen MI, Day SE, Hu D, Neves AA, Gallagher FA, Fulton SM, and Brindle KM (2009). A comparison between radiolabeled fluorodeoxyglucose uptake and hyperpolarized ^{13}C-labeled pyruvate utilization as methods for detecting tumor response to treatment. *Neoplasia* **11**, 574–582.

[34] Casanovas DJ, Hicklin G, Bergers D, and Hanahan D (2005). Drug resistance by evasion of antiangiogenic targeting of VEGF signaling in late-stage pancreatic islet tumors. *Cancer Cell* **8**, 299–309.

[35] Ebos JML, Lee CR, and Kerbel RS (2009). Tumor and host-mediated pathways of resistance and disease progression in response to antiangiogenic therapy. *Clin Cancer Res* **15**, 5020–5025.

[36] Loges S, Mazzone M, Hohensinner P, and Carmeliet P (2009). Silencing or fueling metastasis with VEGF inhibitors: antiangiogenesis revisited. *Cancer Cell* **15**, 167–170.

[37] Dempke WC and Heinemann V (2009). Resistance to EGF-R (erbB-1) and VEGF-R modulating agents. *Eur J Cancer* **45** (7), 1117–1128.

[38] Kerbel RS and Kamen BA (2004). The anti-angiogenesis basis of metronomic chemotherapy. *Nat Rev Cancer* **4**, 425–436.

[39] Jain RK (2005). Normalization of tumor vasculature: an emerging concept in antiangiogenic therapy. *Science* **307**, 58–62.

[40] Alavi A and Basu S (2008). Planar and SPECT imaging in the era of PET and PET-CT: can it survive the test of time? *Eur J Nucl Med Mol Imaging* **35**, 1560–1565.

[41] Fuh G, Wu P, Liang WC, Ultsch M, Lee CV, Moffat B, and Wiesmann C (2006). Structure-function studies of two synthetic anti–vascular endothelial growth factor Fabs and comparison with the Avastin Fab. *J Biol Chem* **281** (10), 6625–6631.

[42] Eppler SM, Combs DL, Henry TD, Lopez JJ, Ellis SG, Yi JH, Annex BH, McCluskey ER, and Zioncheck TF (2002). A target-mediated model to describe the pharmacokinetics and hemodynamic effects of recombinant human vascular endothelial growth factor in humans. *Clin Pharmacol Ther* **72** (1), 20–32.

[43] Sargent DJ, Rubinstein L, Schwartz L, Dancey JE, Gatsonis C, Dodd LE, and Shankar LK (2009). Validation of novel imaging methodologies for use as cancer clinical trial end-points. *Eur J Cancer* **45**, 290–299.